82-1

Publ. Astron. Soc. Japan (2018) 70 (4), 82 (1–6)
doi: 10.1093/pasj/psy077
Advance Access Publication Date: 2018 June 30

Origin of the low-temperature plasma in the Galactic center X-ray emission

Shigeo Yamauchi,[1,*] Miku Shimizu,[1] Masayoshi Nobukawa,[2] Kumiko K. Nobukawa,[1] Hideki Uchiyama,[3] and Katsuji Koyama[4]

[1]Department of Physics, Nara Women's University, Kitauoyanishimachi, Nara, Nara 630-8506, Japan
[2]Faculty of Education, Nara University of Education, Takabatake-cho, Nara, Nara 630-8528, Japan
[3]Faculty of Education, Shizuoka University, 836 Ohya, Suruga-ku, Shizuoka, Shizuoka 422-8529, Japan
[4]Department of Physics, Graduate School of Science, Kyoto University, Kitashirakawa-oiwake-cho, Sakyo-ku, Kyoto, Kyoto 606-8502, Japan

*E-mail: yamauchi@cc.nara-wu.ac.jp

Received 2017 August 18; Accepted 2018 May 30

Abstract

The Galactic Center X-ray emission (GCXE) is composed of high-temperature (∼7 keV) and low-temperature (∼1 keV) plasmas (HTP and LTP, respectively). The global structure of the HTP is roughly uniform over the Galactic Center (GC) region, and the origin of the HTP has been extensively studied. On the other hand, the LTP is more clumpy, and its origin has not been studied in detail. In the S XV Heα line map, a pair of horn-like soft diffuse sources are seen at symmetric positions with respect to Sagittarius A*. The X-ray spectra of the pair are well represented by an absorbed thin thermal plasma model of temperature and $N_{\rm H}$ of 0.6–0.7 keV and $4 \times 10^{22}\,{\rm cm}^{-2}$, respectively. The $N_{\rm H}$ values indicate that the pair are located near the GC. Then the dynamical time scales of the pair are $\sim 10^5$ yr. The Si and S abundances and the surface brightnesses in the S XV Heα line band are 0.7–1.2 and 0.6–1.3 solar, and $(2.0–2.4) \times 10^{-15}\,{\rm erg\,s^{-1}\,cm^{-2}\,arcmin^{-2}}$, respectively. The temperature, abundances, and surface brightness are similar to those of the LTP in the GCXE, while the abundances are far larger than those of known point sources, typically coronal active stars and RS CVn-type active binaries. Based on these results, the possible origin of the LTP is discussed.

Key words: Galaxy: center — X-rays: diffuse background — X-rays: ISM

1 Introduction

The spectrum of the Galactic diffuse X-ray emission (GDXE) has strong K-shell transition lines of highly ionized atoms and neutral iron. The strongest are the He-like iron (Fe XXV Heα) and sulfur (S XV Heα) lines, which indicates that the GDXE is composed of a high-temperature plasma of ∼7 keV (HTP), represented by the Fe XXV Heα line, and a low-temperature plasma of ∼1 keV (LTP), represented by the S XV Heα line (Uchiyama et al. 2013). The other component is a power law with the Fe I Kα line. The equivalent widths and scale heights of the Fe XXV Heα and Fe I Kα lines are position dependent in the GDXE, and hence the GDXE is spatially and spectrally separated into the Galactic Center X-ray emission (GCXE), the Galactic Ridge X-ray emission (GRXE), and the Galactic Bulge X-ray emission (GBXE) (Yamauchi et al. 2016; Nobukawa et al. 2016; Koyama 2018).

A long-standing question for the GDXE is its origin, whether it is the integrated emission of point sources, diffuse plasma, or something else. Using the deep Chandra observation in the 6.5–7.1 keV band, Revnivtsev et al. (2009) and Hong (2012) made an X-ray luminosity function (XLF: the integrated flux of point sources as a function of the point source flux) down to a luminosity of $\sim 4 \times 10^{29}\,\mathrm{erg\,s^{-1}}$, and resolved more than 80% of the flux of the GBXE into point sources. However, the profiles of the XLF and integrated spectra of the point sources were largely different between these authors, which led to different predictions of the point source composition in the GBXE: RS CVn-type active binaries (ABs) and cataclysmic variables (CVs) with a mixing ratio of $\sim$2 : 1 (Revnivtsev et al. 2009), or CVs dominant (Hong 2012). One possibility for this mismatch in the mixing ratio of point sources could be that the authors ignored the energy band difference of the compositions; they simply referred to the XLF results in the 6.5–7.1 keV band (HTP), not the full energy band of the HTP and LTP. Using the spectrum difference of ABs, CVs, and GBXE in the 5–10 keV band, Nobukawa et al. (2016) suggested that the GBXE is composed of ABs and CVs with a mixing ratio of $\sim$3 : 7. In the full energy band (1–10 keV), the compositions would not only be these point sources (ABs and CVs), but may include true diffuse plasma or even unknown objects. Therefore, the simple point source origin should be carefully re-examined for the HTP and LTP in a proper mixture of these two components.

This paper utilizes the GCXE to study the origin of the LTP, because more reliable spectra are available due to the surface brightness being $\sim$10 times larger than the GBXE and GRXE. We report on properties of a pair of soft diffuse sources (denoted as NE and NW) in the LTP map at the northeast and northwest of the Galactic Center (GC). The diffuse sources have been noted by Wang, Gotthelf, and Lang (2002) using Chandra and Ponti et al. (2015) using XMM-Newton, but the detailed information has not been reported. Based on the improved spectral and spatial information from Suzaku, the origin of NE and NW, and a possible interpretation of the origin of the LTP in the GCXE, are discussed. Throughout this paper, the distance to the GC is taken to be 8 kpc (e.g., Reid 1993; Gillessen et al. 2009), and quoted errors are within 90% confidence limits.

2 Observations

Survey observations in the GC region were carried out with the X-ray Imaging Spectrometer (XIS: Koyama et al. 2007) on board Suzaku (Mitsuda et al. 2007). This paper utilizes these Suzaku data from the archive. The XISs are composed of four CCD cameras placed on the focal planes of the thin foil X-ray Telescopes (XRT: Serlemitsos et al. 2007). XIS 1 is a back-side illuminated (BI) CCD, while XIS 0, 2, and 3 are front-side illuminated (FI) CCDs. The field of view (FOV) of the XIS is 17'.8 × 17'.8. Data from three of the sensors (XIS 0, 1, and 3) were used for most of the observations, because XIS 2 stopped working in 2006 November. Since the spectral resolution of the XIS was degraded due to the radiation of cosmic particles, the spaced-row charge injection technique was applied to restore the XIS performance (Uchiyama et al. 2009). After removing hot and flickering pixels, we used data of ASCA grade 0, 2, 3, 4, and 6.

3 Analysis and results

The XIS pulse-height data are converted to pulse-invariant (PI) channels using the `xispi` software in the HEAsoft 6.19 package and the calibration database version 2016-06-07. The data in the South Atlantic Anomaly, during earth occultation, and at the low elevation angles from the earth rim of $<5^\circ$ (night earth) and $<20^\circ$ (day earth) are excluded. Figure 1 shows the results of the Suzaku GC survey, covering the full area of the GC with multiple pointings. The non-X-ray background (NXB), estimated using `xisnxbgen` (Tawa et al. 2008), is subtracted. To highlight the contrast between the HTP and LTP distributions, X-ray images of the Fe XXV Heα (6.55–6.8 keV) and S XV Heα (2.3–2.6 keV) bands were made separately. A pair of soft diffuse sources (NE and NW) are detected in two fields of the XIS. The observation logs of the two fields, which include the pair of sources NE and NW and the background (BGD), are given in table 1.

3.1 Overview of soft diffuse sources in the GCXE

In the Fe XXV Heα line map (HTP distribution), some slight enhancements are found near the giant molecular cloud complex (GMC) of Sagittarius (Sgr) A, Sgr C, and the Arches cluster (blue dashed lines in figure 1a). The Fe XXV Heα line enhancement is $\sim$10% of the GCXE level. Thus, the global distribution of the HTP is smooth in the full area of the GC. In the LTP distribution, on the other hand, the S XV Heα image shows a largely extended X-ray emission near $(l, b) \sim (0^\circ\!.3, 0^\circ\!.4)$ (GC North; Nakashima et al. 2014). The spectrum of this soft diffuse source is in collisional ionization equilibrium (CIE) with a temperature of 0.81 keV and solar abundances. Another soft diffuse source is a super bubble candidate (G359.79−0.26 and G359.77−0.09) found by Mori et al. (2008, 2009) and Heard and Warwick (2013), whose spectra are explained

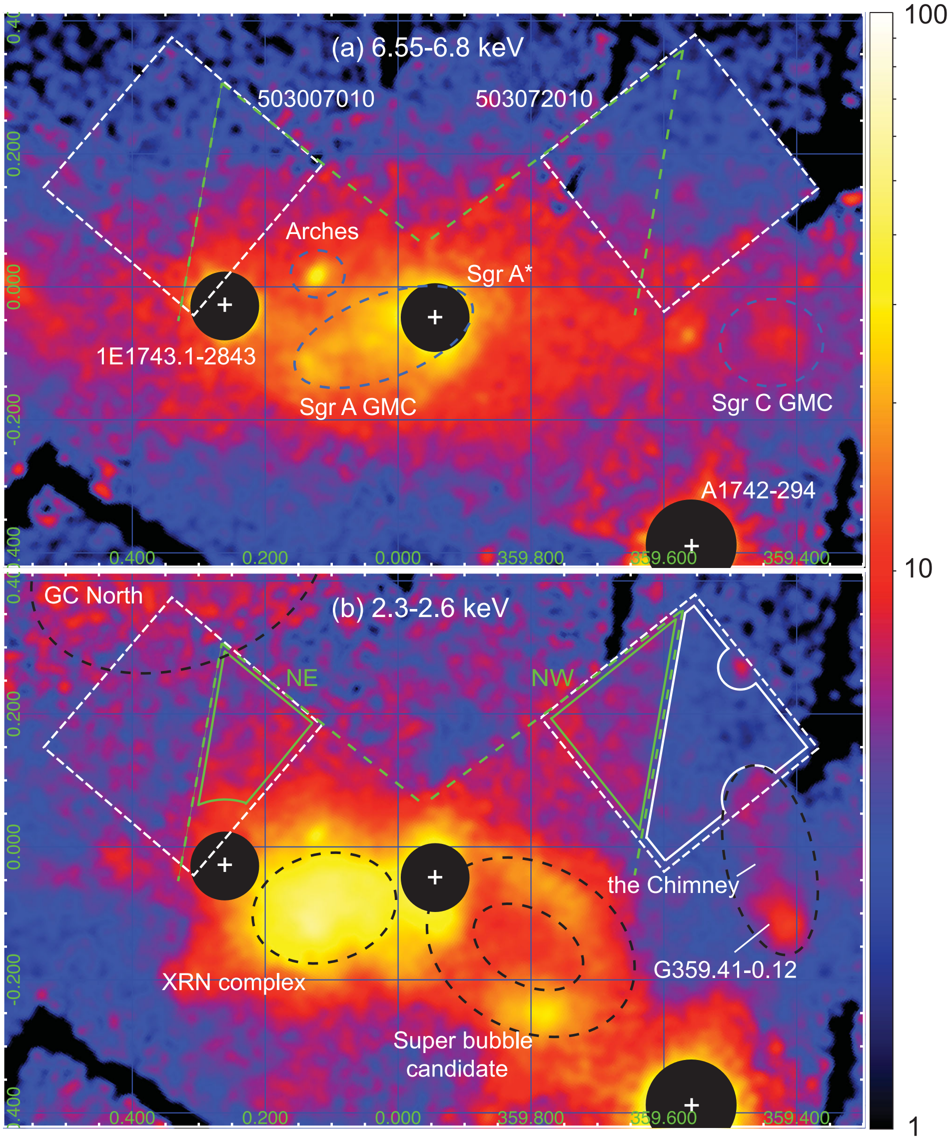

Fig. 1. XIS images in the (a) 6.55–6.8 (Fe XXV Heα) and (b) 2.3–2.6 keV (S XV Heα) bands in the Galactic coordinate. The color bar shows surface brightness in the logarithmic scale. The units are 2×10^{-13} erg s^{-1} cm^{-2} arcmin^{-2} for (a) and 1×10^{-13} erg s^{-1} cm^{-2} arcmin^{-2} for (b). Bright point sources are masked by the black circles. A stray-light region of the brightest source A1742−294 is given by the large black circle. The white dashed squares, the white solid lines, the green solid lines, and the green horn-like lines indicate the XIS FOVs, the background region (BGD), the source regions, and a pair of soft diffuse sources (NE and NW), respectively. The black dashed lines in (b) outline other LTP clumps, while the blue dashed lines in (a) are the regions of HTP clumps. In order to figure out the difference between the HTP and LTP structure, the XIS FOVs and horn-like structures in the LTP are also shown in the HTP image. (Color online)

by an absorbed thermal plasma model in CIE with temperatures of ∼1.0 and ∼0.7 keV, and abundances of 1.1–1.7 and 1.0–1.4 solar, respectively. A notable soft diffuse source is found around the Sgr A X-ray reflection nebula (XRN) near Sgr A* (hear, XRN complex), first reported by Park et al. (2004). This source has a different morphology in the Fe XXV Heα image, slim and faint, which corresponds to the GMC complex (named Sgr A GMC), or Sgr A XRN. For this source, however, no spectral information has been available. Other soft diffuse sources are found near the Sgr C GMC (the Chimney and G359.41−0.12), first reported by Tsuru et al. (2009). The temperatures are ∼1.2 and ∼0.9 keV with abundances of ∼1.7 solar. In addition to these soft diffuse sources, we can see a pair of horn-like diffuse sources, NE and NW, at the north (in the Galactic coordinate) of the GC.

3.2 X-ray spectra of soft diffuse sources, NE and NW

The X-ray spectra of NE and NW after the subtraction of the NXB (see section 2) are made from the source regions.

Table 1. List of data used for spectral analyses.

Observation ID	Pointing position (*l*, *b*)	Observation time (UT) Start–end	Exposure time (ks)	Regions*
503007010	(0°3285, +0°1690)	2008-09-02 10:15:27–2008-09-03 22:52:24	52.2	NE
503072010	(359°5753, +0°1669)	2009-03-06 02:39:12–2009-03-09 02:55:25	140.6	NW, BGD

* See figure 1.

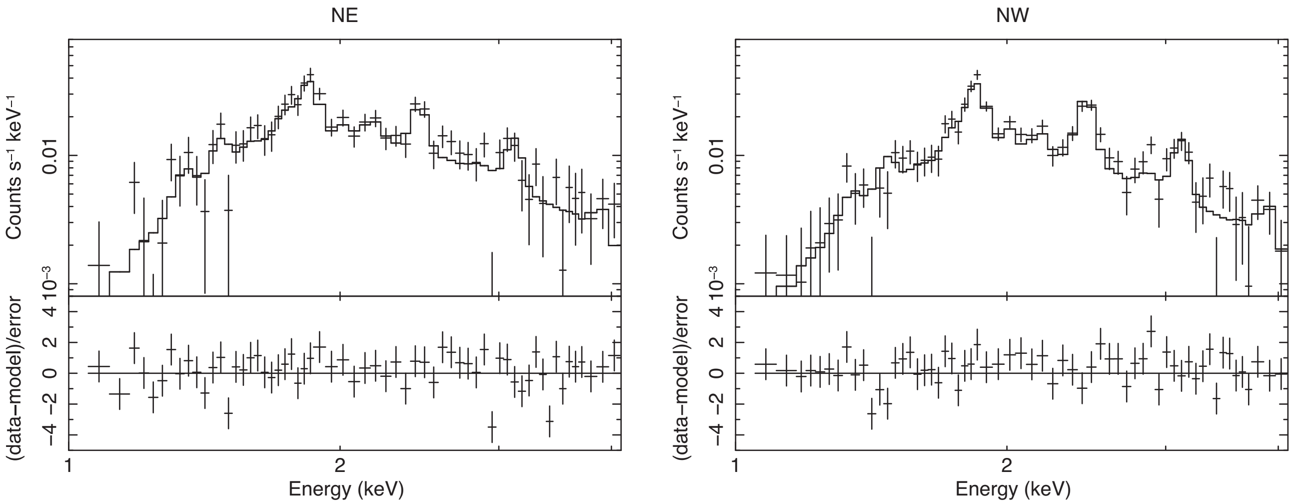

Fig. 2. X-ray spectra of NE and NW (upper panels) and the residuals from the best-fit model (lower panels). Only the spectra obtained with the FI sensors in the 1–4 keV band are displayed for brevity.

The BGD region is selected from a nearby blank sky of similar Galactic latitude to those of NE and NW. The X-ray spectrum of BGD is made with the same process as NE and NW. In order to make the spectra of NE, NW, and BGD with good statistics, we utilize the two XIS fields, which include a large fraction of NE, NW, and BGD, with long exposure times (table 1). The flux of the NXB are ∼9% and ∼14% of the total counts of the background region (BGD) in the 1–8 keV band for FI and BI, respectively, and the statistical error is less then 1%. Thus, the uncertainty caused by the NXB subtraction is not significant in the following spectral analysis. The flux of the BGD spectrum is fine-tuned, taking account of the longitude and latitude differences between BGD and the pair sources (NE and NW), and using the e-folding longitude and latitude scales of the GCXE of 0°63 and 0°26, respectively (Uchiyama et al. 2013; Yamauchi et al. 2016; Koyama 2018). The fine-tuning factor is 1.3 for NE and 1.1 for NW. Then, the BGD spectrum multiplied by this fine-tuning factor is subtracted from the NE and NW spectra. The resultant NE and NW spectra are shown in figure 2, in which many emission line features are found. In order to increase the photon statistics, the spectra with the FI sensors (XIS 0 and 3) are co-added, but the XIS 1 spectrum is treated separately, because the response functions of the FIs and BI are different. Response files, redistribution matrix files (RMFs), and ancillary response files (ARFs) are made using `xisrmfgen` and `xissimarfgen` (Ishisaki et al. 2007), respectively. The abundance tables and the atomic data of the lines and continua of the thin thermal plasma are taken from Anders and Grevesse (1989) and ATOMDB 3.0.9, respectively.

The NE and NW spectra are fitted with a CIE plasma model of solar abundances, `vapec` in XSPEC version 12.9.0u. This model is rejected (χ^2/d.o.f. of 163/119 and 177/119, respectively) with residuals at the Si, S, and Ar lines. Therefore, the NE and NW spectra are re-fitted by the same CIE model, but the abundances of Si, S, and Ar (= Ca) are treated as free parameters. Then an improved fit is obtained with χ^2/d.o.f. of 147/116 and 158/116, respectively.[1] The best-fit model is shown in figure 2, while the best-fit parameters are given in table 2. The fluxes in the S XV Heα line band (2.3–2.6 keV) are 2.4×10^{-15} erg s^{-1} cm^{-2} arcmin^{-2} for NE and 2.0×10^{-15} erg s^{-1} cm^{-2} arcmin^{-2} for NW.

[1] Exactly speaking, this model is not accepted from the statistical point of view, which may be due to systematic errors caused in the BGD subtraction process. Taking account of the possible systematic errors, we regard the model as a good approximation of the NE and NW spectra.

Table 2. Best-fit parameters of NE and NW.

Parameter	Value	
	NE	NW
N_H (cm^{-2})	$(4.4^{+0.3}_{-0.4}) \times 10^{22}$	$(4.2^{+0.6}_{-0.2}) \times 10^{22}$
kT_e (keV)	$0.64^{+0.11}_{-0.07}$	$0.71^{+0.06}_{-0.12}$
Si* (solar)	$0.7^{+0.3}_{-0.2}$	1.2±0.3
S* (solar)	$0.6^{+0.3}_{-0.2}$	1.3±0.3
Ar = Ca* (solar)	2.3±1.1	$3.3^{+1.2}_{-1.1}$
Others* (solar)	1 (fixed)	1 (fixed)
Normalization†	$(4.0^{+2.2}_{-1.5}) \times 10^{-4}$	$(1.7^{+1.6}_{-0.4}) \times 10^{-4}$
χ^2/d.o.f.	147/116	158/116

*Abundance relative to the solar value (Anders & Grevesse 1989).
†Defined as $10^{-14} \times \int n_H n_e dV / 4\pi D^2 \Omega$ (cm^{-5} $arcmin^{-2}$), where n_H, n_e, D, and Ω are hydrogen density (cm^{-3}), electron density (cm^{-3}), distance (cm), and solid angle ($arcmin^2$) of the source, respectively.

4 Discussion

Chandra found many point sources in the GC region (e.g., Muno et al. 2009). The flux of the integrated point sources in the regions of NE and NW is only ~10%, and hence the contribution of the resolved point sources for NE and NW would be negligible. The surface brightness of NE and NW is nearly the same level as the nearby GCXE. The N_H values of the pair of sources, NE and NW, are $\sim 4 \times 10^{22}\,cm^{-2}$ (table 2), roughly consistent with those of the point sources located at the GC region (Sakano 2000; Sakano et al. 2002). Therefore, here and after, we assume that NE and NW are located near the GC region at a distance of 8 kpc.

The pair of soft diffuse sources, NE and NW, have horn-like structures standing above the Galactic plane (see figure 1b). Assuming a cone-shaped geometry with a base diameter of ~15′ (35 pc) and a height of ~15′, the volume (V) is estimated to be $V = 3.3 \times 10^{59}\,cm^3$. Using the best-fit volume emission measure, and assuming a filling factor of 1 and $n_e = 1.2 n_H$, where n_e and n_H are the electron and hydrogen densities, respectively, we obtain the mean hydrogen density (n_H), the thermal energy (E_{th}), gas mass (M_{gas}), and sound velocity (c_s) for NE to be $n_H = 0.3\,cm^{-3}$, $E_{th} = 3 \times 10^{50}$ erg, $M_{gas} = 120\,M_\odot$, and $c_s = 4 \times 10^7\,cm\,s^{-1}$. For NW, we obtain $n_H = 0.2\,cm^{-3}$, $E_{th} = 2 \times 10^{50}$ erg, $M_{gas} = 80\,M_\odot$, and $c_s = 4 \times 10^7\,cm\,s^{-1}$. The dynamical time scale (t_{dyn}) is estimated to be $t_{dyn} \simeq 1 \times 10^5$ yr.

Most of these physical parameters of NE and NW are consistent with those of middle-aged supernova remanants (SNRs). However, the plasma size is larger than typical middle-aged SNRs, and the horn-like morphology is largely different from that of a single SNR. The physical parameters and the dynamical time scales of NE and NW are similar to each other, and the pair positions are symmetric with respect to Sgr A*. These suggest that the pair, NE and NW, originated from the same event, possibly past activity in the GC region.

Remarkable features in the LTP map are the presence of many bright soft diffuse sources (Mori et al. 2008, 2009; Tsuru et al. 2009; Heard & Warwick 2013; Nakashima et al. 2014; Ponti et al. 2015), including NE and NW, near the GC. These soft diffuse sources have similar temperature and Si–S abundances to those of the LTP in the GCXE (Uchiyama et al. 2013). In the scenario of the point source origin for the LTP, a candidate source in the luminosity range of $>10^{30}\,erg\,s^{-1}$ has been regarded to be ABs with a thermal spectrum of temperature $\gtrsim$1 keV (Sazonov et al. 2006; Warwick 2014). However, the fraction of the resolved point sources of the GCXE in this luminosity range is less than a few tens of percent (Muno et al. 2003; Revnivtsev et al. 2007). Therefore, the major contribution of point sources should come from the lowest luminosity range of $\sim 10^{28}$–$10^{30}\,erg\,s^{-1}$. In this luminosity range, the candidate source may not only be ABs, but includes coronal active stars (CAs) with a temperature of $\lesssim$1 keV (e.g., Güdel 2004; Pandey & Singh 2008). In this case, the number of required point sources is more than $\sim 10^5$–10^6, because the total LTP luminosity of the GCXE is $\sim 10^{36}\,erg\,s^{-1}$ (Uchiyama et al. 2013). Since this huge number of point sources would lead a uniform LTP distribution, the presence of many bright soft diffuse sources disfavors the point source origin.

Most of the soft diffuse sources have dynamical time scales of $\sim 10^5$ yr, which corresponds to the last epoch of the high star formation activity of $\sim 10^5$–10^7 yr ago (Yusef-Zadeh et al. 2009). The Si and S abundances of NE and NW and most of the other soft diffuse sources are larger than CAs (typically ~0.2 solar; e.g., Pandey & Singh 2008), but are typical of those of a normal diffuse hot plasma. The horn-like sources NE and NW may be made by either super-wind from multiple supernovae, high activity of stellar wind from many high-mass stars in the GC region $\sim 10^5$ yr ago (Ponti et al. 2015), or the past flares of Sgr A* (e.g., Koyama 2018). The origin of a power-law component with the Fe I Kα line (6.4 keV) would also be the same activities near the GC.

Acknowledgments

The authors are grateful to all members of the Suzaku team. KKN is supported by Research Fellowships of JSPS for Young Scientists. This work was supported by the Japan Society for the Promotion of Science (JSPS) KAKENHI Grant Numbers JP24540232 (SY) and JP16J00548 (KKN).

References

Anders, E., & Grevesse, N. 1989, Geochim. Cosmochim. Acta, 53, 197

Gillessen, S., Eisenhauser, F., Trippe, S., Alexander, T., Genzel, R., Martins, F., & Ott, T. 2009, ApJ, 692, 1075
Güdel, M. 2004, A&AR, 12, 71
Heard, V., & Warwick, R. S. 2013, MNRAS, 434, 1339
Hong, J. 2012, MNRAS, 427, 1633
Ishisaki, Y., et al. 2007, PASJ, 59, S113
Koyama, K. 2018, PASJ, 70, R1
Koyama, K., et al. 2007, PASJ, 59, S23
Mitsuda, K., et al. 2007, PASJ, 59, S1
Mori, H., Hyodo, Y., Tsuru, T. G., Nobukawa, M., & Koyama, K. 2009, PASJ, 61, 687
Mori, H., Tsuru, T. G., Hyodo, Y., Koyama, K., & Senda, A. 2008, PASJ, 60, S183
Muno, M. P., et al. 2003, ApJ, 589, 225
Muno, M. P., et al. 2009, ApJS, 181, 110
Nakashima, S., Nobukawa, M., Uchida, H., Tanaka, T., Tsuru, T. G., Koyama, K., Murakami, H., & Uchiyama, H. 2013, ApJ, 773, 20
Nakashima, S., Nobukawa, M., Uchida, H., Tanaka, T., Tsuru, T. G., Koyama, K., Uchiyama, H., & Murakami, H. 2014, in IAU Symp. 303, The Galactic Center: Feeding and Feedback in a Normal Galactic Nucleus, ed. L. O. Sjouwerman et al. (Cambridge: Cambridge University Press), 349
Nobukawa, M., Uchiyama, H., Nobukawa, K. K., Yamauchi, S., & Koyama, K. 2016, ApJ, 833, 268
Pandey, J. C., & Singh, K. P. 2008, MNRAS, 387, 1627
Park, S., Muno, M. P., Baganoff, F. K., Maeda, Y., Morris, M., Howard, C., Bautz, M. W., & Garmire, G. P. 2004, ApJ, 603, 548
Ponti, G., et al. 2015, MNRAS, 453, 172
Reid, M. J. 1993, ARA&A, 31, 345
Revnivtsev, M., Sazonov, S., Churazov, E., Forman, W., Vikhlinin, A., & Sunyaev, R. 2009, Nature, 458, 1142
Revnivtsev, M., Vikhlinin, A., & Sazonov, S. 2007, A&A, 473, 857
Sakano, M. 2000, Ph.D. thesis, Kyoto University
Sakano, M., Koyama, K., Murakami, H., Maeda, Y., & Yamauchi, S. 2002, ApJS, 138, 19
Sazonov, S., Revnivtsev, M., Gilfanov, M., Churazov, E., & Sunyaev, R. 2006, A&A, 450, 117
Serlemitsos, P., et al. 2007, PASJ, 59, S9
Tawa, N., et al. 2008, PASJ, 60, S11
Tsuru, T. G., Nobukawa, M., Nakajima, H., Matsumoto, H., Koyama, K., & Yamauchi, S. 2009, PASJ, 61, S219
Uchiyama, H., et al. 2009, PASJ, 61, S9
Uchiyama, H., Nobukawa, M., Tsuru, T. G., & Koyama, K. 2013, PASJ, 65, 19
Wang, Q. D., Gotthelf, E. V., & Lang, C. C. 2002, Nature, 415, 148
Warwick, R. S. 2014, MNRAS, 445, 66
Yamauchi, S., Nobukawa, K. K., Nobukawa, M., Uchiyama, H., & Koyama, K. 2016, PASJ, 68, 59
Yusef-Zadeh, F., et al. 2009, ApJ, 702, 178